



OMI total ozone column validation with Aura-AVE CAFS observations

M. Kroon,¹ I. Petropavlovskikh,² R. Shetter,³ S. Hall,³ K. Ullmann,³ J. P. Veefkind,¹
R. D. McPeters,⁴ E. V. Browell,⁵ and P. F. Levelt¹

Received 13 April 2007; revised 26 October 2007; accepted 11 December 2007; published 2 May 2008.

[1] In this paper we present validation results of the total ozone column data products of the Ozone Monitoring Instrument (OMI) by using airborne observations by the CCD Actinic Flux Spectrometer (CAFS) instrument. CAFS was flown during Aura Validation Experiment (AVE) campaigns organized by NASA in support of the validation of EOS-Aura satellite data products. The accuracy of individual CAFS total ozone column estimates of 2.0% on average is sufficient to meet the OMI validation requirements of 3.0%. A climatology was used to estimate the ozone column below the aircraft altitude. AVE validation results show that the OMI-TOMS total ozone column data product is of overall high quality as CAFS and OMI-TOMS agree to within less than 1% with a standard deviation of 8 DU (2–3%) with no significant dependence on total ozone column, latitude, cloud fraction, or solar zenith angle. The primary shortcoming in OMI-DOAS collection 2 total ozone column data is the air mass factor reflected in the dependence on solar zenith angle of the CAFS and OMI-DOAS total ozone column difference. Fortunately, the CAFS aircraft data collected during AVE provided useful insights that could not be obtained in any other way into where OMI satellite data retrieval improvements were needed. For OMI-DOAS collection 3 the air mass factor issue has been solved by calibration optimization and retrieval algorithm improvements, bringing airborne CAFS and OMI-DOAS satellite data to agreement within less than 1.5% with a standard deviation of 9 DU (2–3%), in compliance with the OMI validation requirements.

Citation: Kroon, M., I. Petropavlovskikh, R. Shetter, S. Hall, K. Ullmann, J. P. Veefkind, R. D. McPeters, E. V. Browell, and P. F. Levelt (2008), OMI total ozone column validation with Aura-AVE CAFS observations, *J. Geophys. Res.*, 113, D15S13, doi:10.1029/2007JD008795.

1. Introduction

[2] The Dutch-Finnish Ozone Monitoring Instrument (OMI) [Levelt *et al.*, 2006a, 2006b] aboard the NASA Earth Observing System Aura satellite [Schoeberl *et al.*, 2006] is a compact nadir viewing, wide swath, ultraviolet-visible (270–500 nm) hyperspectral imaging spectrometer that provides daily global coverage with high spatial and spectral resolution. The EOS-Aura orbit is sun-synchronous at 705 km altitude with an ascending node equator-crossing time roughly at 1345 local time. The OMI instrument measures backscattered solar radiance in the dayside portion of each orbit and solar irradiance near the Northern Hemisphere terminator once per day. The OMI satellite data products are derived from the ratio of Earth radiance and solar irradiance and are extensively validated as an essential prerequisite for establishing credibility for satellite data and

subsequent use for scientific research such as continuing the global TOMS total ozone record spanning almost three decades.

[3] The National Aeronautics and Space Agency (NASA) has organized several field campaigns under the name Aura Validation Experiment (AVE) to perform focused measurements of atmospheric species by remote and in situ sensing instruments in support of the validation of EOS-Aura satellite data products. Two of the AVE campaigns were based at Ellington Field, Houston, Texas, USA, from where the majority of flights by the NASA WB-57 aircraft in October/November of 2004 and in June of 2005 covered the Gulf of Mexico and the Midwest U.S. The Polar-AVE campaign held in January/February of 2005 was based at Pease Tradeport, Portsmouth, New Hampshire, USA, from where the NASA DC-8 aircraft performed long-distance flights over snow covered North America, Canada and Greenland. The tropical AVE campaign held in January/February of 2006 took place from Juan Santamaria International Airport in San Jose, Costa Rica, from where the NASA WB-57 aircraft traversed the Pacific Ocean between Costa Rica and the Galapagos Islands, the Caribbean Sea and the Sea of Panama. Both NASA aircraft involved with AVE carried a suite of in situ sampling and remote sensing

¹Royal Netherlands Meteorological Institute, De Bilt, Netherlands.

²Earth System Research Laboratory, NOAA, Boulder, Colorado, USA.

³National Center for Atmospheric Research, Boulder, Colorado, USA.

⁴NASA Goddard Space Flight Center, Greenbelt, Maryland, USA.

⁵NASA Langley Research Center, Hampton, Virginia, USA.

instrumentation that are capable of obtaining correlative observations of columns and profiles of a multitude of atmospheric species in regions of the globe where ground based observations are sparsely available and under atmospheric conditions that pose challenges to satellite data retrievals. With most ground based stations residing in pristine regions, AVE airborne observations provided OMI also with trace gas observations over atmospherically polluted regions that are important for validation [Kroon *et al.*, 2007; McPeters *et al.*, 2002] and science [Levelt *et al.*, 2006a, 2006b], ready for future work.

[4] In this paper we focus on comparing the OMI-TOMS [Bhartia and Wellemeyer, 2002; McPeters *et al.*, 1998] and OMI-DOAS [Veeffkind *et al.*, 2006] total ozone column data products of collection 2 against estimates of total ozone column derived from airborne observations by the CCD Actinic Flux Spectrometer (CAFS) instrument [Petropavlovskikh *et al.*, 2007] during AVE campaigns. The OMI-TOMS algorithm is based on the TOMS V8 algorithm that has been used to process data from a series of four TOMS instruments flown since November 1978. This algorithm uses measurements at 4 discrete 1 nm wide wavelength bands centered at 313, 318, 331 and 360 nm. The OMI-DOAS algorithm [Veeffkind *et al.*, 2006] takes advantage of the hyperspectral feature of OMI. It is based on the principle of Differential Optical Absorption Spectroscopy (DOAS) [Perner and Platt, 1979]. The algorithm uses ~ 25 OMI measurements in the wavelength range 331.1 nm to 336.6 nm, as described by Veeffkind *et al.* [2006]. The key difference between the two algorithms is that the OMI-DOAS algorithm removes the effects of aerosols, clouds, volcanic sulfur dioxide, and surface effects by spectral fitting while the TOMS algorithm applies an empirical correction to remove these effects. In addition, the OMI-TOMS algorithm uses a cloud height climatology that was derived using infrared satellite data, while the OMI-DOAS algorithm uses cloud information derived from OMI measurements in the 470 nm O₂-O₂ absorption band. The two algorithms also respond to instrumental errors very differently. The CAFS instrument measures spectrally resolved actinic flux over a 280 nm to 400 nm wavelength range. From these spectra, estimates of the ozone column above and below the aircraft flight altitude are derived with a dedicated retrieval algorithm [Petropavlovskikh *et al.*, 2007] developed from the traditional Dobson [Hudson and Planet, 1993] or TOMS [McPeters *et al.*, 1998] retrieval methods. Along the flight track the observations by CAFS are compared to spatially and temporally collocated OMI observations by analyzing the total ozone column differences as a function of various parameters relevant to the campaign, such as aircraft altitude, tropospheric ozone climatology and latitude, and parameters relevant to OMI retrievals such as cloud fraction, solar zenith angle, and latitude.

[5] The purpose of this study is to assess the quality of the EOS-Aura satellite-based OMI-DOAS and OMI-TOMS total ozone column data product by comparing the satellite data against estimates of column-integrated (“total”) ozone from airborne observations. Independent correlative measurements of total ozone are critical to establishing confidence and assessing uncertainty in the new OMI measurements, which in turn are critical to continuing the

global total ozone record. First we explain the workings of the CAFS instruments and how total ozone column estimates are obtained. Then we summarize the various AVE deployments and their purpose of probing different geographical regions of the globe where no ground based platform are present, at the same time following the satellite ground track and providing more coincident data points than is available from operational balloon soundings. Following an explanation of our method of comparing satellite and airborne data we present the results obtained from AVE campaigns. These results are checked by verifying the tropospheric ozone climatology used in CAFS retrievals with collocated airborne lidar observations and by analyzing the error budget of individual CAFS observations. Finally, we present an outlook to the new OMI collection 3 data where we demonstrate that various issues identified by means of AVE campaign data in OMI-DOAS collection 2 data have been solved.

2. CAFS Observations and Total Ozone Retrievals

[6] The CCD Actinic Flux Spectroradiometer (CAFS) instruments [Petropavlovskikh *et al.*, 2007] are designed to measure spectrally resolved downwelling or upwelling actinic flux. Photographs of the CAFS instruments in a laboratory environment are presented in Figure 1. The actinic flux optical collector senses photons independent of angle over one hemisphere. The CAFS instruments incorporate Zeiss solid state monochromators and cooled back thinned UV enhanced CCD detectors to detect actinic flux over a wavelength range of 280 nm to 680 nm at 1.6 nm resolution. During the AVE campaigns the wavelength range was limited to the range of 280 nm to 400 nm with an optical filter to improve the stray light rejection of the spectrometer and to enhance the UV short-wavelength measurements. The CAFS instruments flown on the NASA DC-8 and NASA WB-57 platforms were designed to be small, weighing ~ 18 kg each, and have a low power consumption of ~ 8 A of 28 V DC power. On all AVE campaign flights, the same upper and lower CAFS instruments were flown and all performed tests, in the laboratory and in flight, showed a stable calibration and performance.

[7] A dedicated ozone column retrieval algorithm [Petropavlovskikh *et al.*, 2007] is applied to the CAFS measurements taken every 6 s during flight, giving the instrument a possible along-track resolution of about 1200 m on an airplane traveling at 400 kt or 740 km/h. Partial ozone columns are estimated above and below the aircraft’s flight altitude using a Dobson like approach [Hudson and Planet, 1993]. The precision of individual CAFS ozone retrievals is estimated at 1.5–3.3% depending on atmospheric circumstances such as bright surfaces and clouds [Petropavlovskikh *et al.*, 2007]. Despite the investment of considerable effort, it was shown to be difficult to retrieve a sufficiently accurate estimate of the ozone column below the aircraft altitude from the upwelling actinic flux observations because of the variability of clouds, aerosols, and surface reflectivity hampering an accurate determination of the air mass factor. Instead, the 4D TOMS V8 tropospheric ozone climatology was implemented to represent the temporally and spatially resolved ozone profile at the aircraft location from which the partial ozone column below

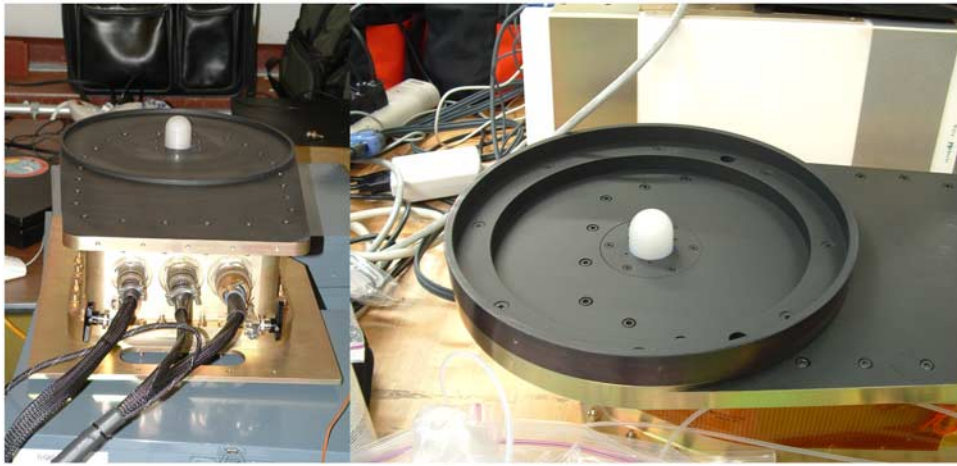


Figure 1. Photographs of the CAFS instrument in the laboratory for the (left) HAVE-1 and (right) HAVE-2 campaigns. The white dome in the center circle is the actinic flux optical collector. To improve the ratio of direct sun over scattered light and to reduce the instrument sensitivity to bright clouds at the horizon, the circular ring has been adopted. (Image courtesy of NCAR.) The ring has been added following the Polar-AVE campaign.

the aircraft altitude can be calculated. Hence, the CAFS total ozone estimates comprises CAFS derived partial ozone columns above the aircraft altitude and climatology based predictions of the ozone column below the aircraft altitude. This climatology, further referred to as “4D climatology,” was produced by C. Wellemeyer and P. K. Bhartia of NASA Goddard Space Flight Center by combining the traditional TOMS V8 ozone profile climatology based on pressure, season, and latitude [McPeters *et al.*, 2007] with a second ozone profile climatology based on pressure, total ozone and latitude, hence the four dimensions. The 4D climatology is a function of total ozone column (125–575 DU, 50 DU increment), latitude (10° averages), month (monthly averages) and altitude pressure (11 Umkehr layers). The pressure at the bottom of an Umkehr layer L amounts to $2^{-(L)} \cdot 1013.25$ hPa, $L = 0, 1, 2, \dots, 10$, where layer 10 extends to 0 pressure. The variance in the ozone sonde data used to calculate the climatological monthly mean ozone profiles is 25% below 30 hPa and 15% above. (According to P. K. Bhartia (private communication, 2007), “The estimate of 25% standard deviation for the tropospheric ozone column is a quite reasonable estimate. The reason why OMI and CAFS may be agreeing better is that OMI doesn’t see the entire tropospheric ozone column, part of it is the same climatology that CAFS uses. Also, even the up-looking CAFS sees some of the ozone below the aircraft through the light reflected off the atmosphere. So there is cancellation of errors. It is quite possible that about half of the error cancels out.”) Ozone sondes have measurement errors of about 5% typically for the troposphere hence we use this error for the monthly mean ozone profiles. The climatological vertical profiles were interpolated to the latitude, month, and OMI-TOMS total ozone, and integrated below the altitude pressure of the aircraft.

[8] Sampling of the 4D climatology requires the OMI-TOMS total ozone column hence the tropospheric climatological ozone should compare well with the tropo-

spheric portion of the data used in the OMI-TOMS total column retrieved data. On the other hand, this helps to get more realistic ozone variability in the troposphere because ozone in the 30–300 hPa altitude range is highly correlated with the total ozone column as the ozone within this altitude range contributes significant weight to the total column. Moreover, the total ozone column derived from OMI measurements has full sensitivity down to 10 km but has only $\sim 50\%$ sensitivity on average to ozone in the lowest 5 km of the troposphere where most tropospheric ozone resides. Unless OMI is over a high reflectivity surface the instrument has very little sensitivity to the lowest 1 km of the troposphere because from down there very few photons make it back up to OMI. This means that tropospheric ozone products derived from OMI will likely have low correlation with boundary layer ozone observations for example performed by the Environmental Protection Agency (EPA).

[9] From observations under various aircraft pitch, roll and yaw motions during the first two AVE deployments, it was observed that a strong contribution of light scattered into a field of the instrument’s view from bright surfaces and low clouds could impact the accuracy of CAFS ozone column retrievals. Following the Polar-AVE campaign, modifications to the up-looking CAFS instrument were made to block its view of the horizon. The “ring” as depicted in Figure 1 was added to better shield the actinic flux detector from the light scattered from bright surfaces below the aircraft altitude and into the actinic flux field of view. Perhaps more importantly, it removes the horizon from the actinic field of view as the horizon is the area with the highest radiative variability. Thus the ozone retrieval error is significantly reduced. This modification was needed for the Costa Rica AVE campaign where the WB-57 flew over bright cloud scenes, and not so much for the Polar-AVE campaign where the DC-8 flew over land cast in twilight. For the June 2005 and January/February 2006 AVE

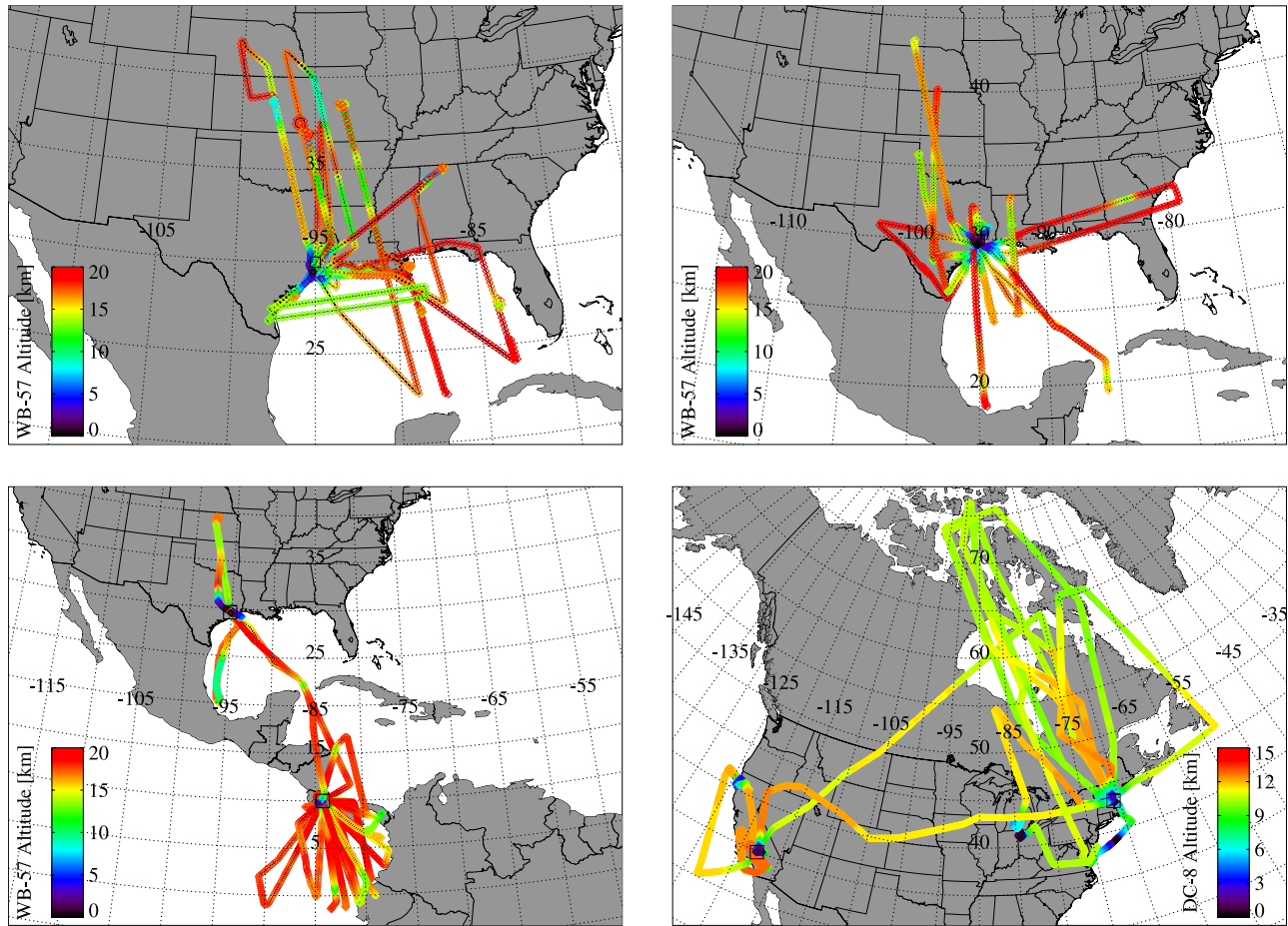


Figure 2. Overview of flights performed by the NASA WB-57 during the (top left) October/November 2004 Houston (HAVE-1), (top right) June 2005 Houston (HAVE-2) and (bottom left) January/February 2006 Costa Rica (CRAVE) AVE deployments and (bottom right) by the NASA DC-8 during the January/February 2005 Portsmouth (PAVE) deployment. Aircraft altitude expressed in kilometers is represented by the color scale. Please note the range in latitude and the various surface types covered per campaign. During Polar-AVE most surface was snow and ice covered.

campaigns the angular response of the instrument was limited by the ring to approximately $\pm 80^\circ$.

3. Airborne Aura Validation Experiment Campaigns

[10] In Figure 2 we present an overview of all AVE campaign flights. The Houston AVE-1 and Houston AVE-2 campaigns, labeled HAVE-1 and HAVE-2 and held in October/November of 2004 and June of 2005, respectively, took place from Ellington Field, Houston, Texas, USA. The NASA WB-57 aircraft 926 performed 5–6 h long flights reaching elevations up to 20 km altitude and covering more than 4000 km of flight track over the Gulf of Mexico and the Midwest U.S.. From this middle latitude deployment site, flights were performed under moderate solar zenith angle conditions, over large-scale cloud fields located above land and ocean, and over cloud free ocean and land surface [Kroon *et al.*, 2004, 2005b]. HAVE-1 campaign flights sampled a range of $+22.6$ to $+41.9^\circ$ in latitude, a range of $+19.1$ to $+84.9^\circ$ in solar zenith angle and were then limited to following the OMI nadir ground pixel

track and the ground tracks of MLS, TES and HIRLDS. HAVE-2 campaign flights sampled a range of $+19.43$ to $+42.94^\circ$ in latitude, a range of $+7.50$ to $+33.10^\circ$ in solar zenith angle and were directed more toward validating EOS-Aura satellite observations over atmospheric phenomena such as tropical storm Arlene.

[11] The Polar-AVE campaign, labeled PAVE, was held in January/February of 2005 and took place from Pease Tradeport, Portsmouth, New Hampshire, USA. The NASA DC-8 aircraft 817 provided a platform for a large payload of scientific equipment for making observations on 8–10 h long flights at altitudes up to 12 km and covering more than 8000 km of flight track over the east coast of the USA and Canada and Greenland. PAVE science flights were performed during local daytime and sampled a range of $+40.83$ to $+70.38^\circ$ in latitude and a range of $+55.30$ to $+90.00^\circ$ in solar zenith angle. PAVE flights sampled the atmosphere under low to very low solar elevation angles where flights crossed the Earth shadow terminator regularly. Ground scenes were snow and ice-covered land and ocean, open ocean, and clouds over snow and ice covered surfaces [Kroon *et al.*, 2005a]. In addition to CAFS, the DIAL

airborne lidar instrument provided information on ozone profiles and the ozone column below the aircraft. PAVE flights were performed following the OMI and MLS ground tracks of subsequent EOS-Aura orbits, explaining the alignment of long-range flights. During two PAVE flights, boundary layer measurements were taken for a short period of time at flight level 1, or 1000 ft above ground level.

[12] The tropical AVE campaign, labeled CRAVE, was held in January/February of 2006 and took place from Juan Santamaria International Airport in San Jose, Costa Rica. Here the NASA WB-57 aircraft 926 covered more than 3500 km of flight track over the Pacific Ocean between Costa Rica, the Galapagos Islands and over the Sea of Panama. Flights from this tropical deployment site provided CAFS with observations at small solar zenith angles. The underlying surface varied between open ocean and open land scenes to various cloud structures such as large cloud decks and high towering cumulus clouds. CRAVE science flights sampled a range of -1.27 to $+27.80^\circ$ in latitude and a range of $+17.40$ to $+60.50^\circ$ in solar zenith angle. The CRAVE campaign provided important information on the differences in treatment of cloudy scenes by the OMI-DOAS and OMI-TOMS total ozone retrieval algorithms via the satellite/CAFS comparisons [Kroon *et al.*, 2006]. Please note that the ranges reported per campaign represent the range of the science flights that have been included in the statistical analysis per campaign.

[13] During HAVE-1 CAFS flew its first science mission where many instrument issues were overcome during the campaign. At the same time the OMI in-flight calibration program was conducted leading to regular OMI level 1B data adjustments. Finally, the OMI-DOAS retrieval algorithm was being developed releasing preliminary data sets. Therefore the results of comparing OMI to HAVE-1 CAFS data are not presented here as both data sets are considered immature. Unfortunately this leads to a scarcity of midlatitude airborne observations because most HAVE-2 measurements are over subtropical regions. However, the comparisons made did reveal the absence of a dependence of the satellite and airborne difference on the satellite total ozone column, solar zenith angle and latitude over the respective range sampled. HAVE-1 thus provided confidence to carry out subsequent CAFS and OMI improvements that were performed independently which has led to obtaining valuable results from the following three AVE campaigns of which the results are presented in this paper.

4. Method of Comparison

[14] All AVE campaign flights were performed during local daytime where the aircraft and EOS-Aura subsatellite tracks were collocated in space and time. Global OMI data of collection 2 is limited to satellite orbits that temporally and spatially overlap with these aircraft tracks. In this paper, the analysis is limited to the OMI-TOMS and OMI-DOAS total ozone estimates obtained from the OMI Science Investigator-led Processing System (OSIPS) of Earth Observing System Data and Information System Core System (ECS) Collection 2. OMI-DOAS data collected between September 2004 and October 2005 was processed with software version v0.9.4. From October 2005 onward v1.0.1 has been operational. OMI-TOMS data has been

processed with the same algorithm for the entire OMI data record. In addition, these satellite data files contain OMI estimates of the cloud fraction and cloud height, and auxiliary information such as time of observation, terrain height, and surface albedo.

[15] The CAFS instrument is designed to be insensitive to the direction of the incoming atmospheric radiation by its design. Hence the signal detected by the upper CAFS instrument could come from anywhere in the upper hemisphere above the aircraft altitude. Solar radiation propagates linearly through the ozone layer and is scattered toward the CAFS instrument mostly in the lower regions of the atmosphere. In this way CAFS receives an ozone layer signal over a fair distance around the aircraft position, here estimated at 40 km. Please note that under most conditions more than half of the CAFS signal is originating from the direct sun observation.

[16] For each CAFS data point, the average of all OMI data points that fall within 40 km from the aircraft position is taken to mimic the way CAFS observes the atmosphere. The results of collocating OMI and CAFS observations are presented as a function of the time difference between the satellite and airborne observations. Furthermore, the difference between the OMI and CAFS total ozone column estimates is analyzed in relation to geometrical and atmospheric parameters such as OMI total ozone column, solar zenith angle, latitude, and cloud fraction. These analyses help to establish the quality of comparisons and to suggest possible improvements to the OMI ozone retrievals.

[17] The distance of 40 km around a given aircraft position captures at most 3 across track and 5 along track neighboring nadir OMI pixels. The average of this data remains to be sensitive for OMI pixels entering and leaving this averaging domain as we basically calculate a moving average along the CAFS data track. Hence spatial variability is likely to be suppressed but certainly not removed or reduced in spatial scale. We have tested whether the distance of 40 km is a fair number. Comparing individual CAFS data points to the nearest OMI pixel yields discontinuities in the OMI data when crossing over between OMI pixels as a flight track remains inside an OMI pixel for a substantial amount of CAFS data points. On the other hand, using an averaging distance of 80 km and more tends to average out the spatial structures as observed by OMI, worsening the comparisons.

5. Results for Polar AVE

[18] Figure 3 presents an example of a typical PAVE campaign flight where we plot the NASA DC-8 flight track as flown on 29 January 2005 over the OMI-DOAS and OMI-TOMS total ozone column fields. The blue time stamps denote Universal Time Coordinated (UTC) flight time on that flight day. Figure 3 indicates that the OMI data orbit was mostly in line with the flight track. Given the duration and spatial range of the PAVE flights, the preceding and following EOS-Aura OMI orbits were also collocated in space and time with portions of a flight track. This particular flight covered EOS-Aura OMI orbit 2890 over a fair range in latitude and associated solar zenith angle while taking onboard measurements close to the daylight terminator and over regions where snow and ice covered land and

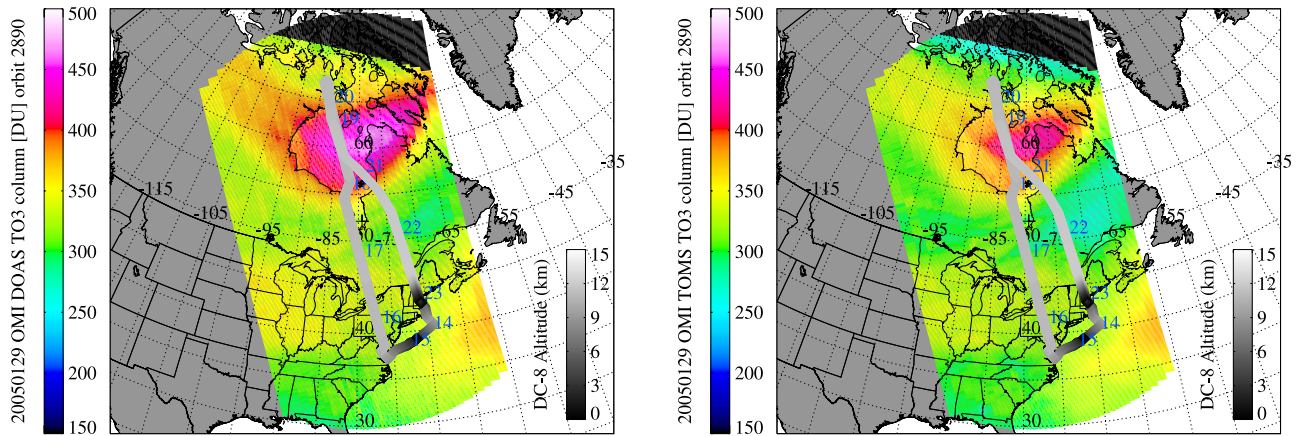


Figure 3. Plotting the PAVE 20050129 (29 January 2005) flight track over the EOS-Aura OMI orbit 2890 total ozone column data products. (left) OMI-DOAS and (right) OMI-TOMS total ozone column. The flight track is gray scale coded by the altitude of flight. The blue numbers accompanying the flight track denote aircraft in-flight time in UTC. Note the higher total ozone column by OMI-DOAS at higher latitudes, e.g., higher solar zenith angle. Also note the low-altitude run over the Atlantic Ocean at flight level 01 (~300 m) and tracking the OMI ground swath over a fair distance. The black region at the top of the OMI orbit is beyond the Earth shadow terminator where no backscattered sunlight is recorded.

ocean surface were typically found. This flight also probed a region of high total ozone column values, where the OMI-DOAS and OMI-TOMS data retrievals provided different estimates of the total ozone column. Atmospheric data recorded under those measurement conditions that pose challenges both satellite and aircraft instrumentation supplied valuable information on the performance of the respective retrieval algorithms. Moreover, the airborne CAFS observations were supported by simultaneous observations from in situ ozone instruments and ozone profile lidar instruments, the latter also provided in-flight information on cloud cover and aerosols.

[19] Figure 4 presents the spatially collocated and averaged OMI data of orbit 2890 and CAFS data taken during the flight depicted in Figure 3. All variables are scaled to the common y axis range. The horizontal axis of Figure 4 represents the time difference in observations taken by the OMI and CAFS instruments. The explanation of the color scheme in Figure 4 is given here and is common for all forthcoming graphs presenting similar results. The gray line denotes OMI cloud fraction data on a 0–100% scale, such that “75” means 75%. The blue line denotes estimates of the ozone column below the aircraft altitude derived from the 4D climatology, given in Dobson units. The red line

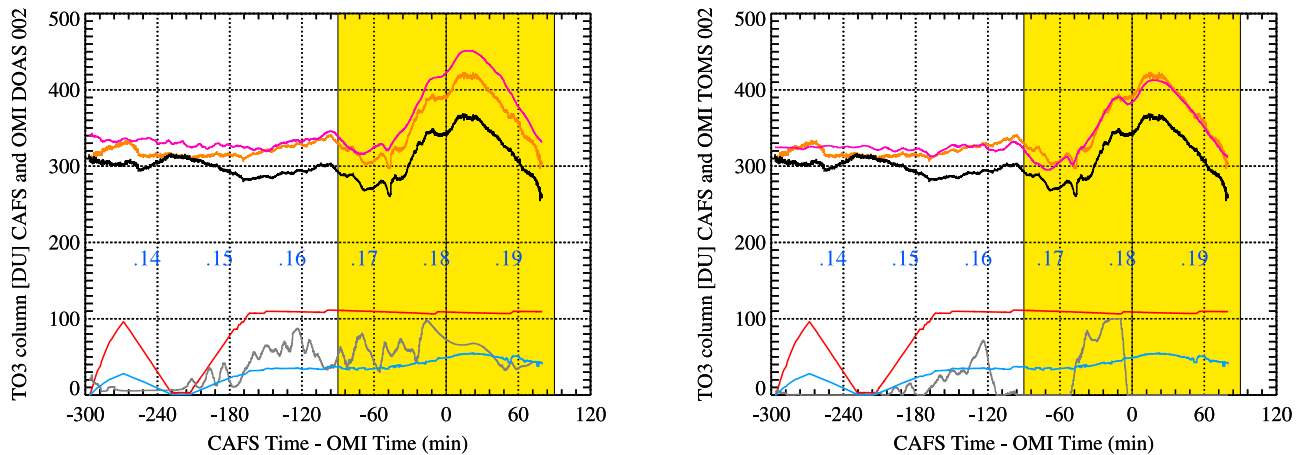


Figure 4. Plotting the CAFS flight 20050129 (29 January 2005) and the collocated EOS-Aura OMI orbit 2890 total ozone column estimates as a function of the time difference of observation. Results for (left) OMI-DOAS and (right) OMI-TOMS total ozone column. Here, from top to bottom, magenta is OMI and orange is CAFS total ozone estimates, black is CAFS stratospheric ozone column estimates, red denotes flight altitude, gray is cloud fraction and blue is the climatological tropospheric ozone column estimate. The blue time stamps denote aircraft in-flight time in UTC at the dot and accompany the flight track depicted in Figure 3. The temporal collocation was restricted to ± 90 min as indicated by the yellow frame. See section 5 for a more elaborate explanation of the common color coding and the scaling of the vertical axis.

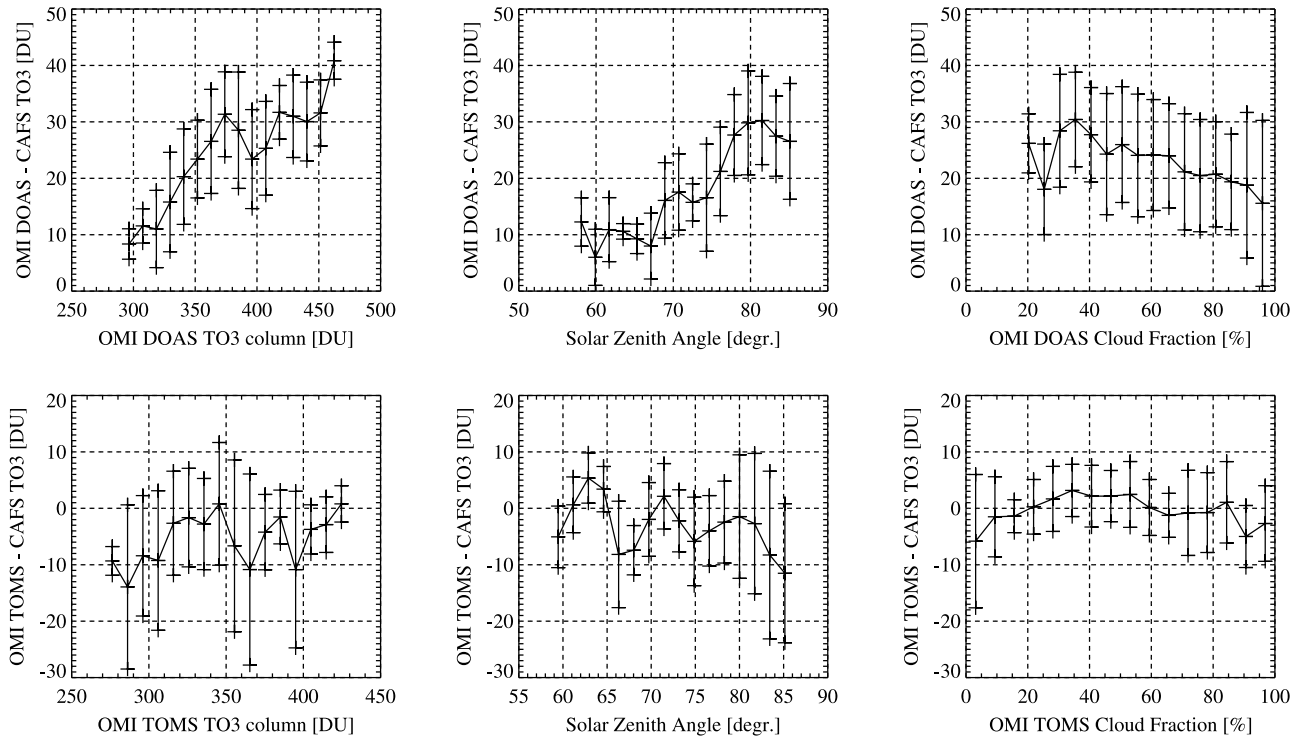


Figure 5. Plotting the difference between OMI and CAFS total ozone column estimates as a function of various observables for all PAVE flights and associated OMI data orbits. Results for (top) OMI-DOAS and (bottom) OMI-TOMS total ozone column estimates. The total ozone column differences are plotted versus (left) total ozone column, (middle) solar zenith angle and (right) cloud fraction. Black vertical lines represent the standard deviation of data points binned in 16 subgroups, while black horizontal lines connect mean offsets calculated for each subgroup.

denotes the altitude of flight on a 100 m scale, such that “115” means 11.500 m. The black line denotes the CAFS-derived ozone column above the aircraft altitude of flight, given in Dobson units. The orange line denotes the CAFS total ozone column estimate that is composed of the CAFS estimate of ozone above and climatological estimate of the ozone below the aircraft altitude; it is marked as the CAFS total ozone column estimate in all results, and is expressed in Dobson units. The magenta line represents the OMI total ozone column data. Blue time stamps denote UTC flight time on that flight day. All collocated OMI data is averaged over a 40 km range centered at the aircraft position. Given the velocity of the EOS-Aura satellite flyby being much greater than the NASA DC-8 aircraft cruising velocity, and on the basis of the stability of the stratosphere, the temporal collocation was restricted to ± 90 min as indicated by the yellow frame.

[20] Figure 4 emphasizes that the CAFS total ozone column estimates of PAVE flight 20050129 and the collocated OMI-TOMS total ozone column measurements of EOS-Aura OMI orbit 2890 are in good agreement. Features of the total ozone fields which are caused by the complicated meteorology of the Northern Hemisphere vortex were captured by both OMI-TOMS and CAFS during this flight. With the NASA DC-8 cruising altitude above the tropopause height of ~ 9 km, the CAFS observed ozone variability can be attributed to the stratosphere. The climatological estimate of ozone below the aircraft shows little structure. The presence of clouds hardly seems to influence the CAFS and OMI-TOMS total ozone column

estimates. At the same time, the comparison of the CAFS and OMI-DOAS total ozone column reveals that a significant offset in total ozone column grows as a function of time that peaks near the coincide point of the aircraft and satellite observations. Following the flight track one observes that the total ozone column difference, commonly defined as OMI minus CAFS, grows with solar zenith angle, latitude, and total ozone column.

[21] Figure 5 presents OMI and CAFS data comparisons as gathered for the entire PAVE campaign as a function of various atmospheric parameters. CAFS observations were made during 8 PAVE flights collocating with 21 EOS-Aura OMI orbits. From left to right Figure 5 presents the total ozone column differences plotted versus total ozone column, solar zenith angle and cloud fraction. Here we do not provide the plot as a function of latitude because total ozone column serves as a good proxy for “equivalent latitude.” Plotting the total ozone column difference as a function of total ozone column also accounts for vortex and jet zonal-ality. Temporal collocation between satellite and aircraft measurements is restricted to ± 90 min. Black vertical lines represent the standard deviation of data points binned in 16 subgroups, while black horizontal lines connect mean offsets calculated for each subgroup. The average difference between OMI-DOAS and CAFS total ozone column estimates over $\sim 13,700$ collocated observations is +24.3 DU with a standard deviation of 10.8 DU. The rather high average difference of 6.7% of the average OMI-DOAS total ozone column is likely caused by the solar zenith angle

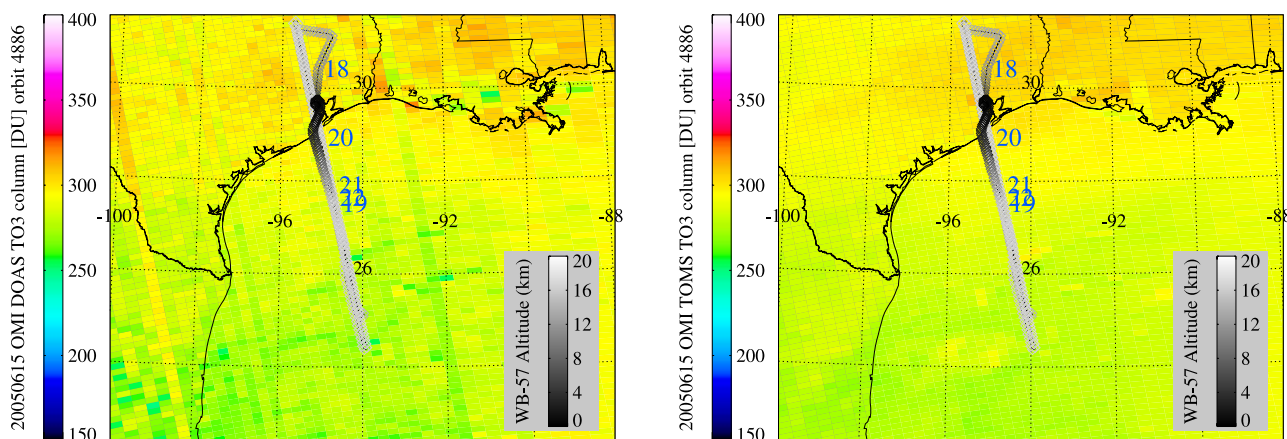


Figure 6. Plotting the HAVE-2 20050615 (15 June 2005) flight track over the EOS-Aura OMI orbit 4886 total ozone column data product. (left) OMI-DOAS and (right) OMI-TOMS total ozone column. Note the presence of more variability on the OMI-DOAS total ozone field as compared to OMI-TOMS as the latter undergoes postprocessing known as soft calibration. The flight track is gray scale coded by the altitude of flight. The blue numbers accompanying the flight track denote aircraft in-flight time in UTC.

dependence of the OMI-DOAS satellite retrieval errors. The average difference between OMI-TOMS and CAFS total ozone column estimates is -3.18 DU, or -0.94% of the average OMI-TOMS total ozone column, with a standard deviation of 9.6 DU. Figure 5 confirms that the OMI-TOMS total ozone column data shows no significant dependence on selected atmospheric parameters, whereas the OMI-DOAS does. All CAFS in-flight data has been processed and assumed to be of equal quality, although in both plots of Figure 5 negative outliers at large solar zenith angle occur. At the time and location of the PAVE campaign, latitude and total ozone column are strongly correlated which provides some explanation for the observed dependencies.

6. Results for Houston AVE-2

[22] Figure 6 presents an example of a typical HAVE-2 campaign flight, where we plot the NASA WB-57 flight track as flown on 15 June 2005 over the OMI-DOAS and OMI-TOMS total ozone column fields of EOS-Aura OMI orbit 4886. Blue time stamps denote UTC flight time on that flight day. Given the duration of NASA WB-57 flights and middle latitude deployment site of the campaign, OMI data is restricted to the single orbit that is covered by the flight track. Preceding and following EOS-Aura OMI orbits were typically not spatially collocated with HAVE-2 flight tracks. This particular flight covers EOS-Aura OMI orbit 4886 while taking ozone data over rural land and open ocean scenes. Note the stronger variability of the OMI-DOAS ozone field compared to OMI-TOMS because for OMI-TOMS correction techniques known as “soft calibration” are applied as a function of cross track position that very effectively reduce striping. Soft calibration is based on the principle that wavelength-dependent calibration can be inferred from the requirement that ozone derived at different wavelengths must be consistent.

[23] Figure 7 presents the spatially collocated and averaged OMI data of orbit 4886 and CAFS data taken during the flight depicted in Figure 6. The color coding of Figure 7

is explained in the previous section. Figure 7 shows that for this particular flight the CAFS and both the OMI-TOMS and OMI-DOAS total ozone column estimates are in agreement, although the selected flight featured a small range of cloud fractions over a small range in total ozone columns. Features of the OMI total ozone fields, followed by the CAFS observations, can be attributed to the stratospheric ozone variability because the altitude of the flight was mostly at 18 km and well above the middle latitude tropopause height. Estimates of ozone column below the aircraft based on the 4D climatology provided little structure in analyzed data. Therefore, small-scale features in the OMI data are probably from the tropospheric ozone variability not captured by the climatology. On the other hand, the climatology appears to represent the actual vertical distribution of tropospheric ozone rather well as the CAFS total ozone column estimate closely follows the satellite data while abruptly changing the aircraft altitude of flight.

[24] Figure 8 summarizes results for all HAVE-2 campaign flight. CAFS observations were made during 8 flights collocated with 8 EOS-Aura OMI orbits. Temporal collocation between satellite and aircraft measurements is here restricted to ± 60 min, as indicated by the yellow frame in Figure 7, which is based on the faster dynamics of the subtropical stratosphere. The average difference between OMI-DOAS and CAFS total ozone column estimates over $\sim 14,600$ collocated observations is $+0.16$ DU, or $+0.06\%$ of the average OMI-DOAS total ozone column, with a standard deviation of 8.9 DU. The average difference between OMI-TOMS and CAFS total ozone column estimates is $+1.36$ DU, or $+0.46\%$ of the average OMI-TOMS total ozone column, with a standard deviation of 8.5 DU. Figure 8 shows that for both OMI-TOMS and OMI-DOAS the comparisons for the HAVE-2 deployment reveal an absence of any dependence on the total ozone column, solar zenith angle and latitude. However, there are clear indications that there is a dependence on cloud fraction found in both satellite data sets. Please note that the achieved results are well within the validation requirements of $\pm 3\%$ for this particular data product [Brinksmas *et al.*,

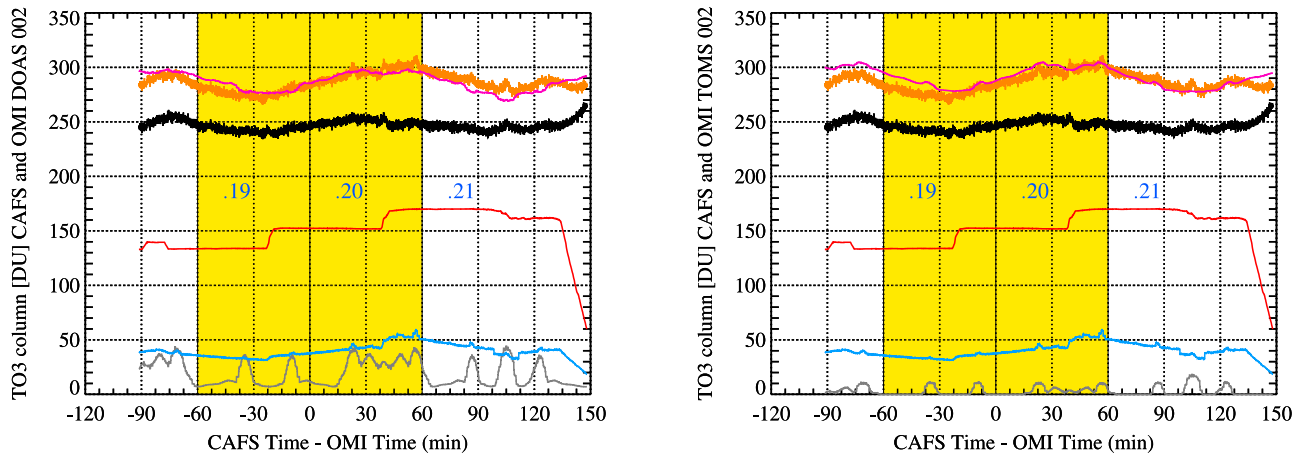


Figure 7. Plotting the CAFS flight 20050615 (15 June 2005) and the collocated EOS-Aura OMI orbit 4866 total ozone column estimates as a function of the time difference of observation. Results for (left) OMI-DOAS and (right) OMI-TOMS total ozone column. See the caption of Figure 4 or the text of section 5 for an explanation of the common color coding and scaling. The blue time stamps denote the aircraft in-flight time in UTC at the dot and accompany the flight track as depicted in Figure 6.

2003]. The large spread of total ozone column differences in all plots represents the variability of satellite and airborne data product retrievals as a function of the range of geophysical conditions sampled, such as clouds, surface albedo, geometric angles and trace gas distributions. How-

ever, it is important to note that variability and uncertainty in the column measurements due to variability in tropospheric/tropopause region ozone and clouds is an important topic of interest because OMI measurements will be used to produce tropospheric ozone residuals, and because this may

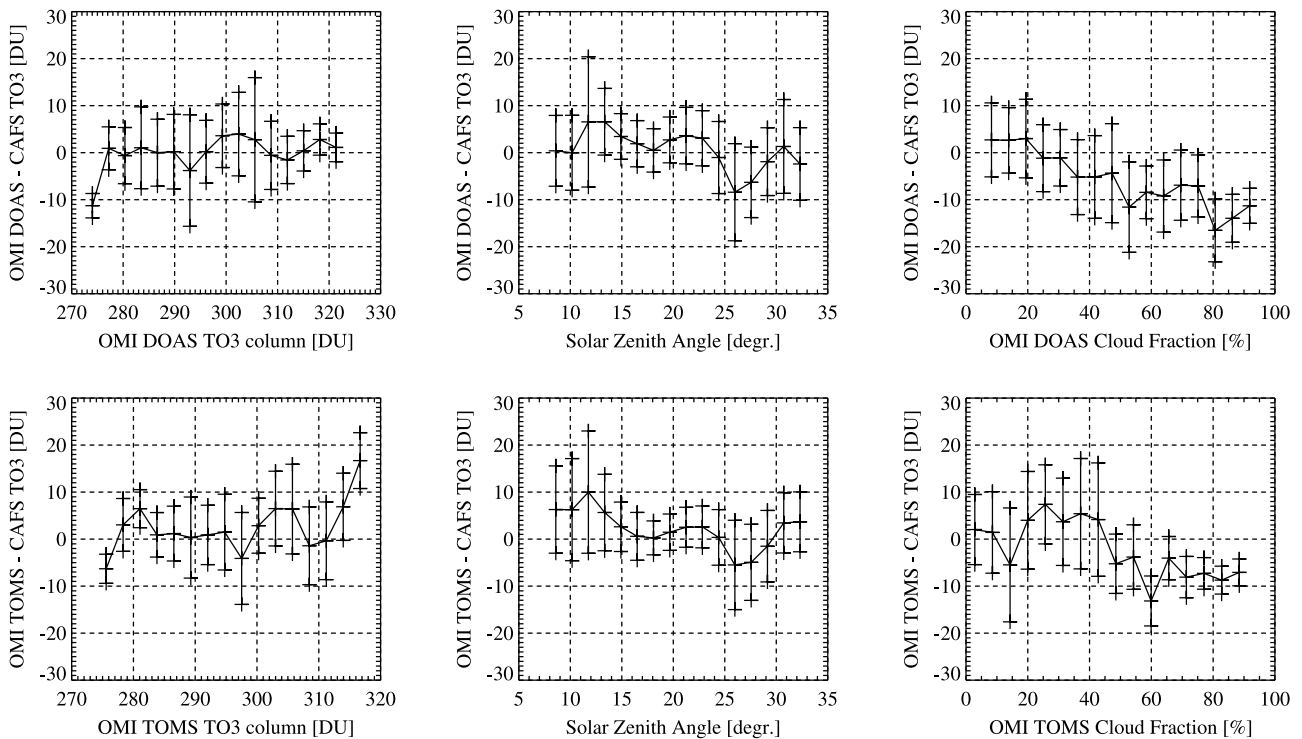


Figure 8. Plotting the difference between OMI and CAFS total ozone column estimates as a function of various observables for all HAVE-2 flights and associated OMI data orbits. Results for (top) OMI-DOAS and (bottom) OMI-TOMS total ozone column estimates. The total ozone column differences are plotted versus (left) total ozone column, (middle) solar zenith angle and (right) cloud fraction. Black vertical lines represent the standard deviation of data points binned in 16 subgroups, while black horizontal lines connect mean offsets calculated for each subgroup.

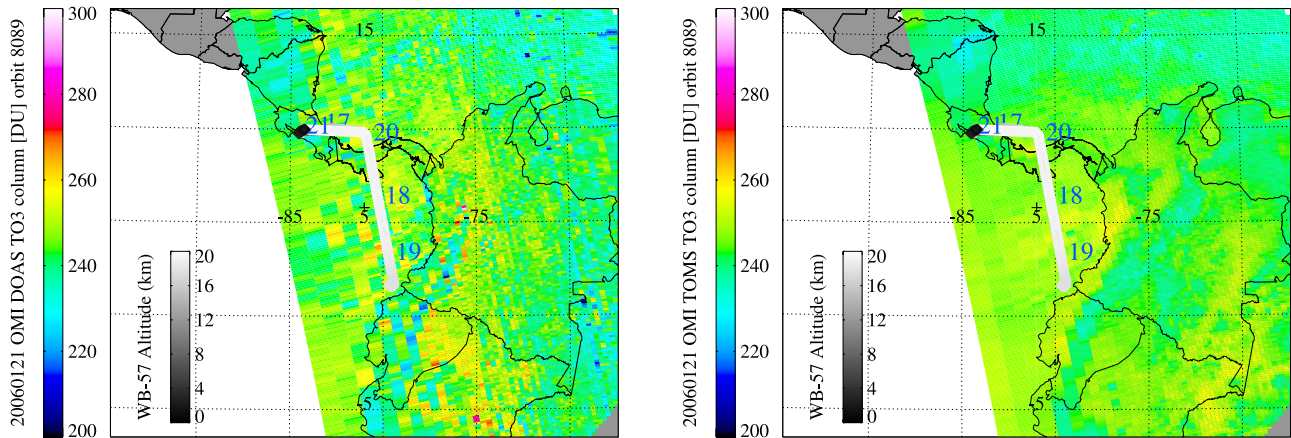


Figure 9. Plotting the CRAVE 20060127 (27 January 2006) flight track over the EOS-Aura OMI orbit 8089 total ozone column data product. (left) OMI-DOAS and (right) OMI-TOMS total ozone column. Note the presence of much more variability on the OMI-DOAS total ozone field as compared to OMI-TOMS as the latter undergoes post processing known as soft calibration. The flight track is gray scale coded by the altitude of flight. The blue numbers accompanying the flight track denote aircraft in-flight time in UTC.

affect evaluation of stratospheric ozone-related dynamics and trends.

7. Results for Costa Rica AVE

[25] Figure 9 presents an example of a typical CRAVE campaign flight, where we plot the NASA WB-57 flight track as flown on 21 January 2006 over the OMI-DOAS and OMI-TOMS total ozone column fields of EOS-Aura OMI orbit 8089. Blue time stamps denote UTC flight time on that flight day. For this tropical deployment, OMI data is restricted to the single orbit that is covered by the flight track. Preceding and following EOS-Aura OMI orbits were typically not spatially collocated with CRAVE flight tracks. This particular flight covers EOS-Aura OMI orbit 8089 mostly over ocean surface. In January, over tropical region,

measurements were made over scenes highly variable in cloud cover and cloud height. With the intertropical convergence zone (ITZC) nearby, cumulus and cumulonimbus clouds were observed to form early in the afternoon. From Figure 9 one observes a larger variability of the OMI-DOAS ozone field as compared to OMI-TOMS. Moreover, clear features of reduced total ozone in Figure 9 indicate measurements over high elevations of the Andes Mountains. However, for OMI-TOMS correction techniques known as “soft calibration” are applied as a function of cross track position that very effectively reduce striping.

[26] Figure 10 presents the spatially collocated and averaged OMI data of orbit 8089 and CAFS data taken during the flight depicted in Figure 9. In the tropics the dynamics of the total ozone field is rather calm, explaining the smooth OMI ozone data seen in Figure 10. Both satellite

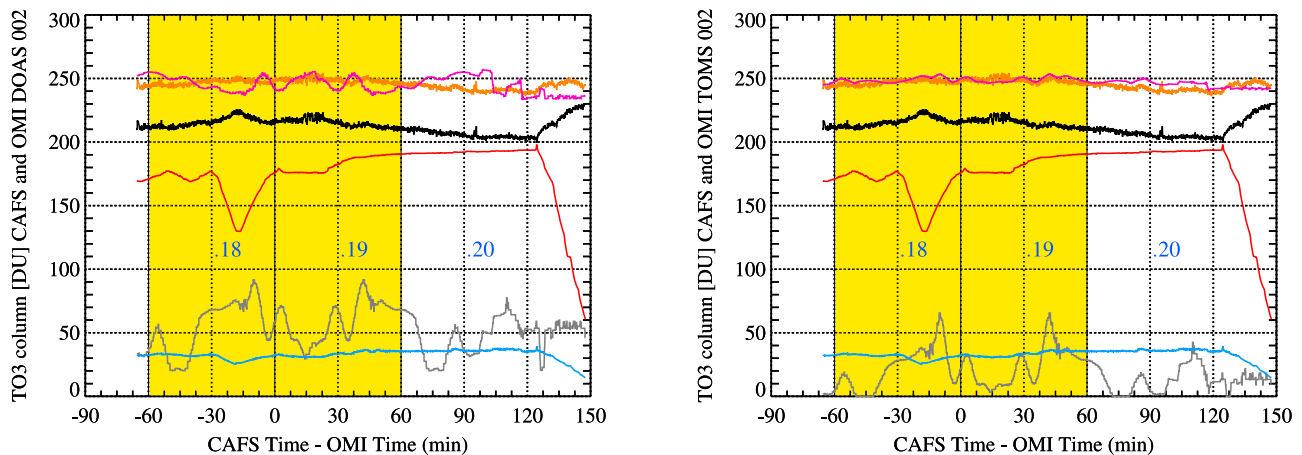


Figure 10. Plotting the CAFS flight 20060127 (27 January 2006) and the collocated EOS-Aura OMI orbit 8089 total ozone column estimates as a function of the time difference of observation. Results for (left) OMI-DOAS and (right) OMI-TOMS total ozone column. See the caption of Figure 4 or the text of section 5 for an explanation of the common color coding. The blue time stamps denote the aircraft in-flight time in UTC at the dot and accompany the flight track as depicted in Figure 9.

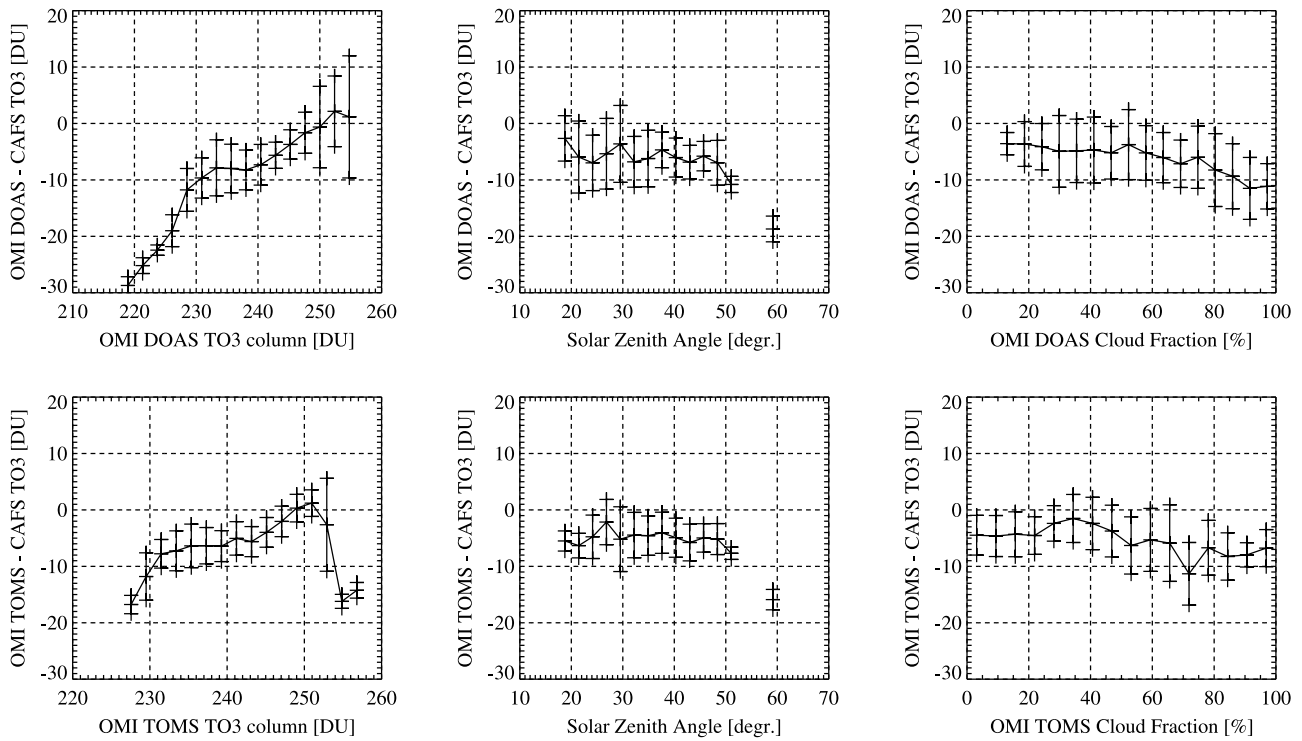


Figure 11. Plotting the difference between OMI and CAFS total ozone column estimates as a function of various observables for all CRAVE flights and associated OMI data orbits. Results for (top) OMI-DOAS and (bottom) OMI-TOMS total ozone column estimates. The total ozone column differences are plotted versus (left) total ozone column, (middle) solar zenith angle and (right) cloud fraction. Black vertical lines represent the standard deviation of data points binned in 16 subgroups, while black horizontal lines connect mean offsets calculated for each subgroup.

data products seem to compare well with the airborne observations.

[27] Figure 11 summarizes results for all CRAVE campaign data. CAFS observations were made during 12 flights covering 12 EOS-Aura OMI orbits. Temporal collocation is restricted to ± 60 min. The average difference between OMI-DOAS and CAFS total ozone column estimates over $\sim 11,400$ collocated observations is -5.70 DU, or -2.36% of the average OMI-DOAS total ozone column, with a standard deviation of 5.4 DU. The average difference between OMI-TOMS and CAFS total ozone column estimates is -4.55 DU, or -1.87% of the average OMI-TOMS total ozone column, with a standard deviation of 4.3 DU. Figure 11 suggests that for both the OMI-TOMS and OMI-DOAS total ozone retrievals the comparisons against CAFS total ozone estimates lack any evidence of a correlation with either solar zenith angle, cloud fraction or latitude variables. However, there are clear indications that residuals show a dependence on the total ozone column in both versions of the OMI retrieved data. Even so, the final numbers are well within the validation requirements of $\pm 3\%$ for the OMI total ozone column data product [Brinksma *et al.*, 2003].

8. Results for AVE Campaigns Combined

[28] Analysis of validation results across the AVE campaigns has shown difficulty in drawing firm conclusions from individual flights. Comparisons between satellite and airborne observations are apparently obscured by

uncertainties such as instrumental noise, inaccuracies such as retrieval errors and calibration issues, and geometric considerations such as aircraft maneuvering and cloud fraction. Combining all observations from one dedicated campaign has shown that an improvement of the statistics is achieved and that trends and correlations become more apparent. The next logical step is to collect all data recorded during all AVE campaigns and analyze the difference between OMI and CAFS as a function of several atmospheric variables as discussed above. However, this step can only be undertaken when all data involved is trustworthy, i.e., that the intercampaing performance of the CAFS instruments is stable and reliable and that the OMI collection 2 total ozone data is of a continuous quality.

[29] Figure 12 summarizes the results for all AVE campaigns except for HAVE-1. Temporal collocation was restricted to ± 60 min, or the lower limit of stability of the stratosphere. The average difference between OMI-DOAS and CAFS total ozone column estimates over $\sim 35,800$ collocated observations is $+5.10$ DU, or $+1.71\%$ of the average OMI-DOAS total ozone column, with a standard deviation of 15.0 DU. The average difference between OMI-TOMS and CAFS total ozone column estimates is -1.2 DU, or -0.62% of the average OMI-DOAS total ozone column, with a standard deviation of 8.3 DU. The results of combined AVE comparisons highlight an excellent agreement between the CAFS and OMI-TOMS retrieved total ozone estimates. Figure 12 also reveals that the difference between the CAFS and OMI-DOAS total

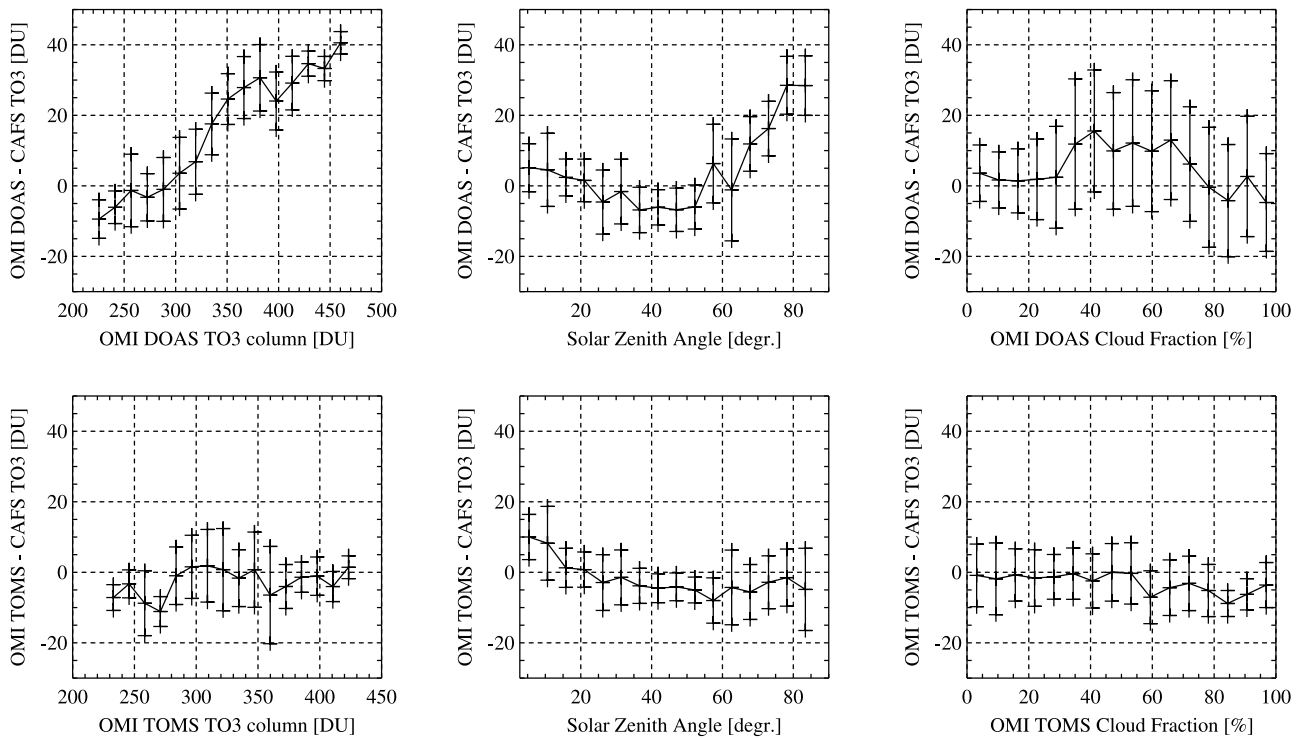


Figure 12. Plotting the difference between OMI and CAFS total ozone column estimates as a function of various observables for all AVE flights and associated OMI data orbits. Results for (top) OMI-DOAS and (bottom) OMI-TOMS total ozone column estimates. The total ozone column differences are plotted versus (left) total ozone column, (middle) solar zenith angle and (right) cloud fraction. Black vertical lines represent the standard deviation of data points binned in 16 subgroups, while black horizontal lines connect mean offsets calculated for each subgroup.

ozone column observations relates to the OMI-DOAS total ozone column estimates. The same behavior is observed in the plots of the differences against the latitude. On the other hand, the latitude and total ozone column are strongly correlated, which provides some explanation for the observed latitude correlations. Similarly, the solar zenith angle is related to the latitude of the observation, which can explain the observed correlations during the PAVE campaign.

[30] Despite capturing a wide range of cloud fraction values, there is no clear evidence for a correlation between the CAFS and OMI total ozone column differences and the OMI cloud fraction data. However, comparisons of the OMI-DOAS and OMI-TOMS total ozone estimates have revealed a strong dependence on cloud height [Kroon *et al.*, 2008]. The OMI-TOMS retrieval relies on predictions from cloud height climatology derived from infrared and microwave observations. The OMI-DOAS retrieval implements the OMI O₂-O₂ cloud data product for estimates of actual cloud height. These numbers are found to strongly vary per cloud scene and hence the ghost column estimates vary as well. The OMI-TOMS combination of cloud height climatology and tropospheric ozone climatology is more compatible with the use of the 4D climatology by CAFS retrievals. This explains in part the larger spread in the comparisons for the OMI-DOAS data product. All in all, the spread in comparisons is most likely caused by combining all detected cloud scenes in a single plot.

[31] Analysis and comparisons of OMI-TOMS and OMI-DOAS total ozone column estimates [Kroon *et al.*, 2008] have shown that OMI-DOAS is not sensitive to the presence of clouds in OMI ground pixels largely because actual OMI O₂-O₂ effective cloud height data is used to determine the ozone “ghost” column below the clouds. With respect to OMI-DOAS, OMI-TOMS total ozone column estimates are biased 5–10 DU higher or lower because of the presence of clouds with effective cloud heights much lower or higher, respectively, than prescribed by the cloud height climatology. Examples are cumulonimbus systems in the ITCZ, hurricanes and tropical cyclones. However, under most cloud conditions the effect is small because there the climatological approach works. CAFS retrievals of the ozone column above the aircraft altitude are somewhat sensitive to the presence of clouds below, at 1–2% on average, depending on the aircraft altitude above the cloud deck altitude and the cloud deck thickness. However, most cruising flight altitudes were well above the clouds decks, flight planning was tuned to cover clear skies or areas where uniform cloud decks were expected and the CAFS detection system was modified to block its view of the bright horizon. In summary we expect no significant effect of clouds on the average difference between OMI and CAFS total ozone column estimates, however, some effect on the standard deviation is feasible. The reasoning above also explains the absence of a clear dependence on OMI cloud fraction of the average difference between OMI and CAFS total ozone column estimates.

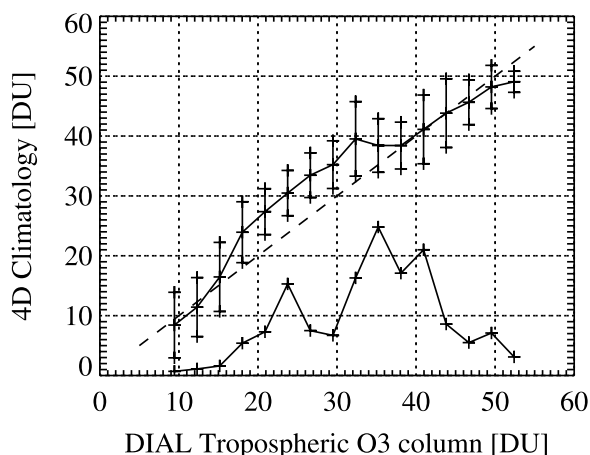


Figure 13. Plotting the estimates of ozone column below the aircraft altitude by the 4D climatology as a function of collocated DIAL observations for all PAVE flights. Black vertical lines represent the standard deviation of data points binned in 16 subgroups, while black horizontal lines connect mean offsets calculated for each subgroup. The dashed line denotes a 1:1 match between the climatological and DIAL. The lower dotted line represents the number of 4D Climatology-DIAL pairs per subgroup scaled by a factor 10 (such that “20” means 200 pairs).

[32] During PAVE various flights crossed the Northern Hemisphere polar jet stream while during HAVE the Northern Hemisphere subtropical jet stream was crossed on occasion. Atmospheric jet streams may cause structures in ozone fields both in horizontal and vertical directions as a result of (1) atmospheric circulations caused by the jet’s flow and rotation and (2) seasonal drifting of the jet’s position and altitude [Cuevas *et al.*, 2007]. OMI total ozone column estimates are expected not to be sensitive to vertical displacements over limited distances of ozone concentrations by the jet streams rotation as vertical profile density variations are integrated into the total ozone column estimate. Horizontal variations on spatial scales larger than OMI pixels as caused by the jet streams are considered to represent true data where variations on spatial scales smaller than OMI pixels are averaged out. Most CAFS estimates of the ozone column above the aircraft altitude would not be influenced by the presence of the jet streams as the aircraft involved were mostly flying well above the jet stream core altitude, located in the upper troposphere. However, estimates of tropospheric ozone columns from the 4D TOMS climatology could in principle be influenced by the jet streams as the climatology, representing a long-term average over several years with varying jet stream conditions, does not represent the actual and variable position of jet streams. At the same time, sampling of the 4D climatology requires the OMI-TOMS total ozone column as a boundary condition and hence the tropospheric climatological ozone estimate should compare well with the true tropospheric portion of the total ozone column (see section 2). This mechanism may well represent the actual jet stream influence on the tropospheric ozone column and hence the total ozone column estimates by CAFS. Hence we expect no significant effect of the jets streams on the average difference between

OMI and CAFS total ozone column estimates whereas effects on the standard deviation are feasible.

9. Verifying Tropospheric Ozone Climatology With Lidar Measurements

[33] During the PAVE campaign the UV Differential Absorption Lidar (DIAL) instrument flew aboard the NASA DC-8. The DIAL instrument performed time-resolved measurements of backscattered pulsed laser light at three wavelengths from which profile information on aerosols, clouds, and ozone above and below the aircraft was retrieved. Vertical integration of the retrieved volume mixing ratios from ground level up to the aircraft altitude provided independent estimates of the ozone column below the aircraft. This vertical integration was performed only for cloud free observations and with low aerosol loading. However, the CAFS and DIAL observations were performed on different time grids. For each CAFS data point, the nearest DIAL measurement in time within a $1^\circ \times 1^\circ$ box in space is chosen to avoid comparing CAFS and DIAL data that are too far apart. DIAL estimates of the ozone column below the aircraft altitude were compared with climatological ozone estimates. The 4D climatology was used to obtain estimates of ozone column below the aircraft level with respect to the altitude, latitude, and season of the CAFS measurements.

[34] Figure 13 shows the pairs of the DIAL estimates of the ozone column below aircraft altitude and the 4D climatology matched to the CAFS observations as plotted for all flights of the Polar AVE campaign. The plotted data cover the aircraft altitude range of 8–12 km, which results in 1486 collocated observations. The black vertical lines in Figure 13 represent the standard deviation of the data points binned in 16 subgroups, while black horizontal lines connect mean offsets calculated for each subgroup. Figure 13 shows that the DIAL observation and the samples of the 4D climatology matched to the CAFS observations tend to correlate well. Linear regression yields a slope of 0.72 and a vertical axis intersection of 12.5 DU, hence the pairs do not match one to one over the entire range of the data. However, the bulk of the measured data points fall within the range of 30–50 DU. Our results indicate that the 4D climatology is in fairly good agreement with the DIAL estimates above 35 DU, while below 35 DU the climatology tends to overestimate tropospheric ozone by about 10 DU with respect to the DIAL observations. The small uncertainties represented by the error bars tend to confirm good agreement.

10. Verifying Tropospheric Ozone Climatology With Satellite Data

[35] Satellite data retrievals apply climatologies to account for the part of the atmosphere obscured by clouds. For each ground pixel, OMI trace gas data is the combination of a measured part as extracted from the measured Earth reflectance and a modeled part based on cloud information and tropospheric trace gas climatologies. The same method applies to the CAFS total column estimates; the ozone column above the aircraft altitude is derived from CAFS upward looking actinic flux measurement and the

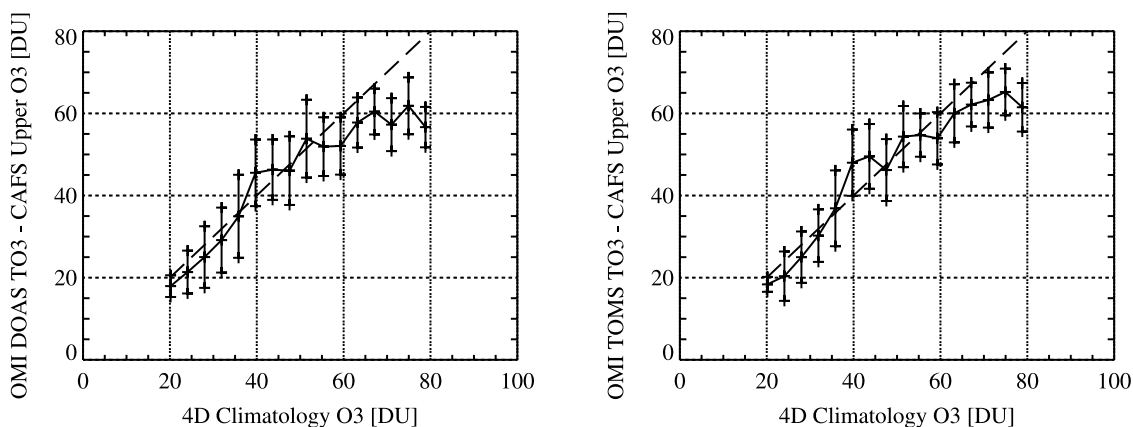


Figure 14. Plotting the difference of OMI total ozone column estimates minus the CAFS estimates of the ozone column above the aircraft as a function of the 4D climatology samples. Results for (left) OMI-DOAS and (right) OMI-TOMS. Black vertical lines represent the standard deviation of data points binned in 16 subgroups, while black horizontal lines connect mean offsets calculated for each subgroup. Dashed line denotes the 1:1 match. For OMI-DOAS the linear regression coefficient amounts to 0.857 with an offset of 0.16. For OMI-TOMS the comparison is even better, where the linear regression coefficient amounts to 0.919 with an offset of 2.64.

part below the aircraft altitude is obtained from the 4D climatology. Assuming the CAFS partial ozone column above the aircraft to be accurate, subtracting this partial ozone column from the OMI total ozone column estimates yields the OMI ozone column below the aircraft altitude. When these residuals are comparable to the subset of the 4D climatology matched to the aircraft data in both space and time, the 4D climatology is considered to be representative from the satellite perspective.

[36] In Figure 14 we plot the OMI-based estimate of the ozone column below the aircraft as a function of the 4D climatological estimate. Here we limit the discussion to the HAVE-2 and CRAVE campaign data because the solar zenith angle dependence of OMI-DOAS as seen from PAVE is a retrieval error that will introduce artifacts. Data has been limited to OMI cloud fractions smaller than 20%. Black vertical lines represent the standard deviation of data points binned in 16 subgroups, while black horizontal lines connect mean offsets calculated for each subgroup. The dashed line denotes the ideal match. From Figure 14 we conclude that there clearly exists a good correlation between the two estimates of the ozone column below the aircraft. For OMI-DOAS the linear regression coefficient amounts to 0.857 with an offset of 0.16. For OMI-TOMS the comparison is even better, where the linear regression coefficient amounts to 0.919 with an offset of 2.64. The linear regression coefficients close to unity confirm the quality of the comparison. Therefore, we conclude that the climatologies used for comparisons of the airborne and satellite data are representative of tropospheric ozone to a high degree.

11. Accuracy of CAFS Total Ozone Estimates

[37] The accuracy of the CAFS total ozone column estimates obtained by adding the CAFS upper instrument partial column observations and the tropospheric ozone climatology is derived from the accuracy of the two terms.

[38] For the PAVE campaign the partial ozone column estimates from CAFS ozone retrievals have an accuracy upper estimate of 1.8% [Petrovavlovskikh *et al.*, 2007] in the presence of clouds or over snow at high solar zenith angle conditions and a 1.5% [Petrovavlovskikh *et al.*, 2007] accuracy upper estimate over cloud free dark surfaces at high solar zenith angle conditions. Low sun conditions and cruising altitude of the DC-8 at 10–12 km were typical for the PAVE campaign hence the numbers are representative for the altitude and SZA range covered. For the HAVE-2 campaign CAFS observations were performed under moderate solar zenith angle conditions, mostly no clouds yielding 2.8% uncertainty and occasional clouds yielding 3.3% uncertainty. On average a RMS 3.0% accuracy estimate for CAFS data during HAVE-2 is obtained. For the CRAVE campaign the errors are even smaller, about 1.7% for cloudy conditions and 2.1% for clouds free conditions. On average a RMS 1.9% accuracy estimate for CAFS data during CRAVE is obtained.

[39] The largest contribution to this accuracy/uncertainty is the sensitivity of the retrieval to the ozone profile shape, which was provided by coincident MLS profiles. For the spatially and temporally collocated estimate from the 4D climatology of the tropospheric ozone column below the aircraft, an error of about 5% is assumed on the basis of the typical error in the tropospheric portion of ozonesonde data [Smit *et al.*, 2007; Johnson *et al.*, 2002].

[40] From the Polar-AVE CAFS data set we obtain an average total ozone column of ~ 340 DU, an average tropospheric ozone column below the aircraft altitude (~ 10 km) of ~ 40 DU and hence ~ 300 DU for CAFS derived averaged ozone above the aircraft altitude. Weighing the reported accuracies with the average contributions normalized to the average total ozone column and taking the normalized root mean square value, following;

$$\text{accuracy} = \sqrt{\left(\frac{[40 * 5.0]^2 + [300 * 1.8]^2}{\sqrt{(40^2 + 300^2)}}\right)},$$

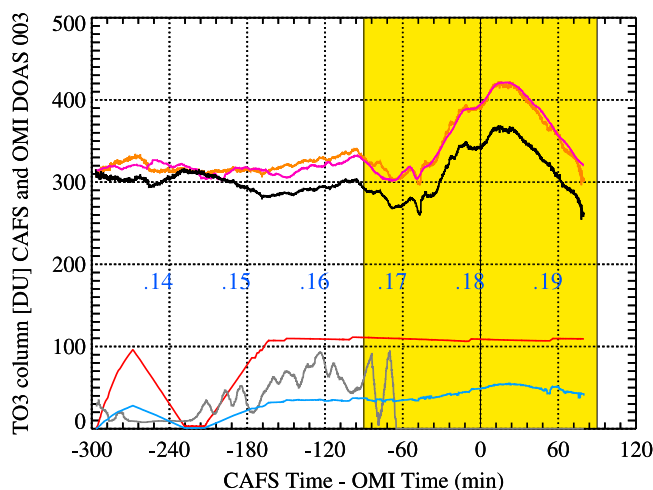


Figure 15. Plotting the CAFS flight 20050129 (29 January 2005) and the collocated EOS-Aura OMI orbit 2890 OMI-DOAS collection 3 total ozone column estimates as a function of the time difference of observation. See the caption of Figure 4 or the text of section 5 for further explanation and interpretation. The blue time stamps denote the aircraft in-flight time in UTC at the dot and accompany the flight track as depicted in Figure 3.

yields an accuracy of 1.9%. During the HAVE-2 and CRAVE campaigns slightly lower averaged total ozone values are reported where the tropospheric contribution is slightly higher compared to PAVE. Working with an average total ozone column of ~ 300 (~ 245) DU, an average tropospheric ozone column below the aircraft altitude of ~ 15 km of ~ 50 (~ 30) DU and hence ~ 250 (215) DU for CAFS derived averaged ozone above the aircraft altitude for HAVE-2 (CRAVE), one obtains an accuracy of 3.1% (2.0%) with the respective error numbers stated above for these campaigns.

12. Outlook to OMI Collection 3 Total Ozone Column Data

[41] On the basis of a continuous effort for improving the quality and understanding of the OMI instrument calibration by performing in-flight calibration investigations, the OMI calibration team has delivered a data set of optimal instrument settings for the entire OMI data record [Dobber *et al.*, 2008]. With this data set all OMI level 0 data will be reprocessed toward a new collection of OMI level 1B data and subsequent to OMI level 2 data that will be labeled collection 3. Major improvements of this level 1B collection are (1) optimized radiometric calibration settings, (2) improved dark current corrections and (3) improved stray light corrections. In addition, the level 2 retrieval algorithms will be optimized on the basis of validation results obtained with collection 2. For the OMI-DOAS total ozone column retrieval the most important changes are (1) a new air mass factor table to incorporate the spherical shape of the atmosphere and (2) a new scheme to deal with snow and ice covered surfaces. As part of testing these new developments, OMI level 2 DOAS total ozone column collection 3 data was calculated for the Polar-AVE time period.

[42] Figure 15 presents the spatially collocated and averaged OMI-DOAS collection 3 data of EOS-Aura OMI orbit 2890 and CAFS data taken during the 20050129 PAVE

flight. Contrary to the results obtained with collection 2, Figure 15 shows that OMI-DOAS and CAFS total ozone column estimates tend to follow each other accurately for the entire data record of this flight. When comparing Figure 15 to Figure 4 (left), we conclude that the comparison of the OMI-DOAS collection 3 and the OMI-TOMS collection 2 total ozone columns are on a par. Figure 16 summarizes the result of comparing CAFS data to OMI-DOAS collection 3 data for the entire PAVE campaign. Temporal collocation was restricted to ± 90 min. The average bias between the $\sim 13,700$ pairs of satellite and airborne total ozone column estimates amounts to +3.4 DU, or a mere 1% of the average OMI-DOAS data. These results are improved from the original bias of +24.1 DU obtained with OMI collection 2 data. New results are also much closer to the -3.2 DU bias based on the OMI-TOMS data comparisons. The standard deviation of residuals found between the matched OMI collection 3 and CAFS data is 10.6 DU, which is similar to the 10.8 DU standard deviation of residuals found between the matched OMI-TOMS and CAFS total ozone estimates.

[43] Figure 16 shows that the overall trends reported in all plots of Figure 5 are strongly suppressed. Moreover, the solar zenith angle dependence found in the above discussed analysis of the OMI-DOAS collection 2 has been strongly reduced. As a result, the above mentioned dependence of satellite-aircraft residuals on latitude and total ozone column has also been strongly reduced. Furthermore, the spread in the analyzed residuals has been greatly reduced which is indicative of the increased maturity of the satellite retrieval algorithm in handling clouds in combination with bright surfaces.

13. Conclusions

[44] The AVE airborne observations were well timed with the discoveries of issues related to the air mass factor in the OMI-DOAS retrieval and with issues related to the cloud

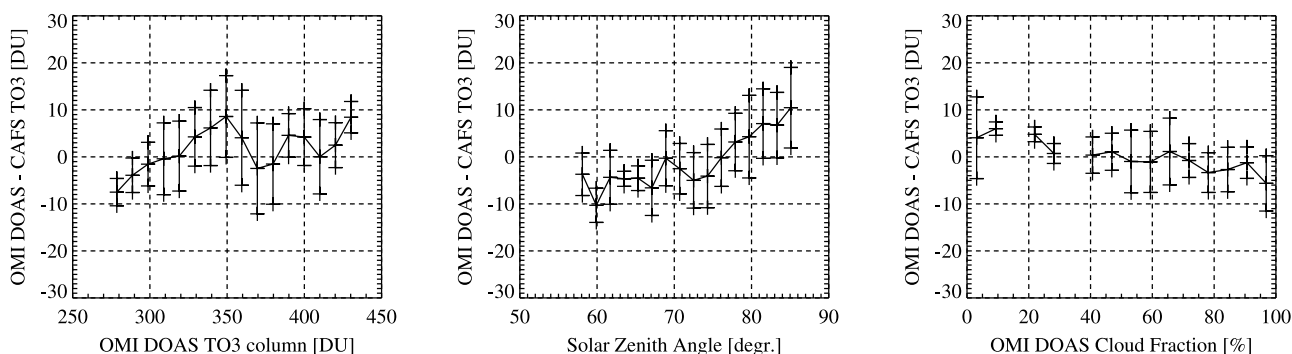


Figure 16. Plotting the difference between OMI-DOAS collection 3 and CAFS total ozone column estimates as a function of various observables for all PAVE flights and associated OMI data orbits. The total ozone column differences are plotted versus (left) total ozone column, (middle) solar zenith angle and (right) cloud fraction. Black vertical lines represent the standard deviation of data points binned in 16 subgroups, while black horizontal lines connect mean offsets calculated for each subgroup. Note the improved agreement between satellite and airborne data as compared to Figure 5.

pressure climatology in the OMI-TOMS retrieval [Kroon *et al.*, 2008]. During Polar-AVE the DC-8 probed the Northern Canada polar regions under measurements conditions posing challenges to both the OMI and the CAFS total ozone column retrieval algorithms. During HAVE-1, HAVE-2 and CRAVE the WB-57 provided correlative observations under clear and moderately cloudy conditions at midlatitudes and over high towering clouds in the tropics. HAVE-1 data made it clear that improvements to the calibration of CAFS and the retrieval of partial ozone columns from CAFS actinic flux data were needed and here the comparisons with the satellite data provided useful clues. Subsequent AVE campaigns provided a wealth of CAFS data of sufficient quality to pinpoint shortcomings in the OMI-DOAS satellite data and to confirm the quality of OMI-TOMS satellite data.

[45] The statistical analysis of all campaign data, except HAVE-1 data, shows that OMI-TOMS is performing well within the OMI validation requirement specifications, at least for the stratosphere since a climatology is used for the troposphere. CAFS and OMI-TOMS agree to within less than 1.0% with a standard deviation of 8–9 DU (2–3%), the latter presumably being all stratospheric or measurement noise due to using a tropospheric climatology and performing measurements above clouds. This standard deviation does not decrease significantly when all AVE missions are compiled. The effect of clouds is a good topic for future work, given an estimated magnitude of 5–10 DU, comparable to the tropospheric and stratospheric uncertainties individually.

[46] On the other hand, the OMI-DOAS collection 2 total ozone columns referenced against the CAFS estimates revealed a strong correlation with the solar zenith angles, an observation which agrees with the conclusions drawn from validating OMI-DOAS ozone column data against ground based data [Balis *et al.*, 2007]. The results presented in that paper show a globally averaged agreement of better than 1% for OMI-TOMS data and better than 2% for OMI-DOAS data with ground-based observations by Dobson and Brewer spectrophotometer instruments. The OMI-TOMS data product is shown to be of high overall quality with no significant dependence on solar zenith angle

or latitude. For the OMI-DOAS data product a significant dependence on solar zenith angle is found when referenced to the ground-based data.

[47] Fortunately, collocated OMI and CAFS observations during Polar-AVE provided useful insights into where satellite data retrieval improvements were needed as detailed information on atmospheric and surface conditions was readily available. The OMI-DOAS total ozone column retrieval algorithm has subsequently been improved in handling snow and ice covered surfaces under cloud free and cloudy conditions. Furthermore, the improved retrieval algorithm processed preliminary OMI level 1B collection 3 spectral data set of limited time span and generated with optimized calibration settings. The validation results for the Polar-AVE campaign dramatically improved, from an offset of 24.3 DU, or 6.7%, with a standard deviation of 10.8 DU to a mere 3.4 DU, or 1.0%, with a standard deviation of 10.6 DU when progressing from collection 2 to 3. On the basis of these introductory results we conclude that the combination of calibration optimization adjustments and retrieval algorithm improvements has largely overcome the shortcomings identified with the OMI-DOAS collection 2 data.

[48] The success of the AVE aircraft program relies on obtaining multiple coincident correlative data points collected during flights along and across the satellite ground tracks as compared to the much smaller number of coincidences typically found in balloon sounding data, on probing regions of the globe where no ground based platform are readily available and covering much more ground track than balloon soundings ever would, and on tuning flight plans to cover those geophysical conditions that remain to pose challenges to the retrieval of atmospheric satellite data products. For any future satellite mission it is therefore highly recommended to perform correlative measurement from airborne platforms aimed at collecting information valuable for validation and essential for answering retrieval challenges that could not be obtained in any other way.

[49] **Acknowledgments.** The authors wish to thank the large team of people responsible for the enormous amount of work in planning and implementing aircraft field missions needed to make the DC-8 and WB-57 validation flights during the AVE deployments so very successful for validating the new satellite instruments on EOS-Aura. In particular we

wish to thank David Fahey of NOAA Earth System Research Laboratory, Eric Jensen of NASA Ames Research Center, and Paul Newman and Mark Schoeberl of NASA Goddard Space Flight Center. The authors wish to thank NASA headquarters for their essential support for these important validation flights. In particular we wish to thank Michael Kurylo (Upper Atmospheric Research Program Manager), Hal Maring (Radiation Science Program Manager) and Phil DeCola (EOS-Aura Program Scientist). The Dutch-Finnish built OMI instrument is part of the NASA EOS-Aura satellite payload. The OMI project is managed by NIVR and KNMI in the Netherlands. The OMI-TOMS and OMI-DOAS total ozone data were obtained from the NASA Goddard Earth Sciences (GES) Data and Information Services Center (DISC), home of the GES Distributed Active Archive Center (DAAC). To obtain KNMI OMI documents, please visit our Web site. AVE related documents can be found under "NASA Campaigns." The OMI validation requirements document and the White Paper can be found under "Requirements." The detailed OMI validation handbook can be found under "Validation Handbook." Please visit <http://www.knmi.nl/omi/research/validation> or send your request to mark.kroon@knmi.nl.

References

- Balis, D., M. Kroon, M. E. Koukouli, E. J. Brinksma, G. Labow, J. P. Veefkind, and R. D. McPeters (2007), Validation of Ozone Monitoring Instrument total ozone column measurements using Brewer and Dobson spectrophotometer ground-based observations, *J. Geophys. Res.*, *112*, D24S46, doi:10.1029/2007JD008796.
- Bhartia, P. K., and C. Wellemeyer (2002), TOMS-V8 total O₃ algorithm, in *OMI Ozone Product, OMI-ATBD-02*, vol. II, edited by P. K. Bhartia, pp. 15–31, NASA Goddard Space Flight Cent., Greenbelt, Md.
- Brinksma, E. J., F. Boersma, and P. F. Levelt (2003), OMI validation requirements document, *KNMI Doc. RS-OMIE-KNMI-345*, R. Neth. Meteorol. Inst., De Bilt, Netherlands.
- Cuevas, E., J. J. Rodriguez, M. Gil, J. C. Guerra, A. Redondas, and J. J. Bustos (2007), Stratosphere-troposphere exchange processes driven by the subtropical jet, paper presented at 7th Annual Meeting, Eur. Meteorol. Soc., San Lorenzo de El Escorial, Spain, 1–5 Oct.
- Dobber, M. R., Q. Kleipool, R. Dirksen, P. Levelt, G. Jaross, S. Taylor, T. Kelly, and L. Flynn (2008), Validation of Ozone Monitoring Instrument level 1b data products, *J. Geophys. Res.*, doi:10.1029/2007JD008665, in press.
- Hudson, R. D., and W. G. Planet (Eds.) (1993), Handbook for Dobson ozone data re-evaluation, *Global Ozone Res. and Monit. Proj. Rep. 29, WMO/TD 597*, World Meteorol. Organ., Geneva, Switzerland.
- Johnson, B. J., S. J. Oltmans, H. Vomel, H. G. J. Smit, T. Deshler, and C. Kroger (2002), Electrochemical concentration cell (ECC) ozonesonde pump efficiency measurements and tests on the sensitivity to ozone of buffered and unbuffered ECC sensor cathode solutions, *J. Geophys. Res.*, *107*(D19), 4393, doi:10.1029/2001JD000557.
- Kroon, M., E. J. Brinksma, and R. D. McPeters (2004), OMI validation opportunities for the AVE October 2004 validation campaign, Ellington Field, Houston, TX, USA, *KNMI Doc. PL-OMIE-KNMI-652*, R. Neth. Meteorol. Inst., De Bilt, Netherlands, Oct.
- Kroon, M., E. J. Brinksma, and R. D. McPeters (2005a), OMI validation opportunities for the AVE January 2005 validation campaign, Pease Tradeport, Portsmouth, NH, USA, *KNMI Doc. PL-OMIE-KNMI-653*, R. Neth. Meteorol. Inst., De Bilt, Netherlands.
- Kroon, M., E. J. Brinksma, and R. D. McPeters (2005b), OMI validation opportunities for the AVE June 2005 validation campaign, Ellington Field, Houston, TX, USA, *KNMI Doc. PL-OMIE-KNMI-654*, R. Neth. Meteorol. Inst., De Bilt, Netherlands.
- Kroon, M., R. D. McPeters, and E. J. Brinksma (2006), OMI validation opportunities for the AVE January 2006 validation campaign, San Jose Airport, Costa Rica, *KNMI Doc. PL-OMIE-KNMI-655*, R. Neth. Meteorol. Inst., De Bilt, Netherlands.
- Kroon, M., E. J. Brinksma, P. K. Bhartia, and R. D. McPeters (2007), EOS-Aura Ozone Monitoring Instrument validation priorities, *KNMI Doc. SN-OMIE-KNMI-723*, R. Neth. Meteorol. Inst., De Bilt, Netherlands.
- Kroon, M., J. P. Veefkind, M. Sneep, R. D. McPeters, P. K. Bhartia, and P. Levelt (2008), Comparing OMI-TOMS and OMI-DOAS total ozone column data, *J. Geophys. Res.*, doi:10.1029/2007JD008798, in press.
- Levelt, P. F., G. H. J. van den Oord, M. R. Dobber, A. Malkki, H. Visser, J. de Vries, P. Stammes, J. O. V. Lundell, and H. Saari (2006a), The Ozone Monitoring Instrument, *IEEE Trans. Geosci. Remote Sens.*, *44*(5), 1093–1101, doi:10.1109/TGRS.2006.872333.
- Levelt, P. F., E. Hilsenrath, G. W. Leppelmeier, G. H. J. van den Oord, P. K. Bhartia, J. Tamminen, J. F. de Haan, and J. P. Veefkind (2006b), Science objectives of the Ozone Monitoring Instrument, *IEEE Trans. Geosci. Remote Sens.*, *44*(5), 1199–1208, doi:10.1109/TGRS.2006.872336.
- McPeters, R. D., et al. (1998), *Earth Probe Total Ozone Mapping Spectrometer (TOMS) data products user's guide*, NASA Tech. Publ. 1998–206895, 70 pp., NASA Goddard Space Flight Cent., Greenbelt, Md.
- McPeters, R. D., P. K. Bhartia, J. F. de Haan, and P. F. Levelt (2002), White Paper on OMI science goals and validation needs, *KNMI Doc. SN-OMIE-KNMI-405*, R. Neth. Meteorol. Inst., De Bilt, Netherlands.
- McPeters, R. D., G. J. Labow, and J. A. Logan (2007), Ozone climatological profiles for satellite retrieval algorithms, *J. Geophys. Res.*, *112*, D05308, doi:10.1029/2005JD006823.
- Perner, D., and U. Platt (1979), Detection of nitrous-acid in the atmosphere by differential optical-absorption, *Geophys. Res. Lett.*, *6*, 917–920, doi:10.1029/GL006i012p00917.
- Petropavlovskikh, I., R. Shetter, S. Hall, K. Ullmann, and P. K. Bhartia (2007), Algorithm for the charge-coupled-device scanning actinic flux spectroradiometer ozone retrieval in support of the Aura satellite validation, *J. Appl. Remote Sens.*, *1*, 013540.
- Schoeberl, M. R., et al. (2006), Overview of the EOS-Aura mission, *IEEE Trans. Geosci. Remote Sens.*, *44*(5), 1066–1074, doi:10.1109/TGRS.2005.861950.
- Smit, H. G. J., et al. (2007), Assessment of the performance of ECC-ozonesondes under quasi-flight conditions in the environmental simulation chamber: Insights from the Juelich Ozone Sonde Intercomparison Experiment (JOSIE), *J. Geophys. Res.*, *112*, D19306, doi:10.1029/2006JD007308.
- Veefkind, J. P., J. F. de Haan, E. J. Brinksma, M. Kroon, and P. F. Levelt (2006), Total ozone from the Ozone Monitoring Instrument (OMI) using the OMI-DOAS technique, *IEEE Trans. Geosci. Remote Sens.*, *44*(5), 1239–1244, doi:10.1109/TGRS.2006.871204.
- E. V. Browell, NASA Langley Research Center, Hampton, VA 23681-2199, USA.
- S. Hall, R. Shetter, and K. Ullmann, National Center for Atmospheric Research, 1850 Table Mesa Drive, Boulder, CO 80305, USA.
- M. Kroon, P. F. Levelt, and J. P. Veefkind, Royal Netherlands Meteorological Institute, P.O. Box 201, NL-3730 AE De Bilt, Netherlands. (mark.kroon@knmi.nl)
- R. D. McPeters, NASA Goddard Space Flight Center, Code 916, Greenbelt, MD 20771, USA.
- I. Petropavlovskikh, Earth System Research Laboratory, NOAA, 325 Broadway, Boulder, CO 80305, USA.